

# The dynamical transition in proteins and non-Gaussian behavior of low frequency modes in Self Consistent Normal Mode Analysis

Jianguang Guo<sup>1</sup>, Timo Budarz<sup>2</sup>, Joshua M. Ward<sup>3</sup>, and Earl W. Prohofsky\*<sup>1</sup>

<sup>1</sup>Department of Physics, Purdue University, West Lafayette, IN 47907

<sup>2</sup>Department of Physical Science, Santa Ana College, Santa Ana, CA 92706

<sup>3</sup>Department of Medicinal Chemistry and Molecular Pharmacology, West Lafayette, IN 47907

## Abstract

Self Consistent Normal Mode Analysis (SCNMA) is applied to heme c type cytochrome f to study temperature dependent protein motion. Classical Normal Mode Analysis (NMA) assumes harmonic behavior and the protein Mean Square Displacement (MSD) has a linear dependence on temperature. This is only consistent with low temperature experimental results. To connect the protein vibrational motions between low temperature and physiological temperature, we have incorporated a fitted set of anharmonic potentials into SCNMA. In addition, Quantum Harmonic Oscillator (QHO) theory has been used to calculate the displacement distribution for individual vibrational modes. We find that the modes involving soft bonds exhibit significant non-Gaussian dynamics at physiological temperature, which suggests it may be the cause of the non-Gaussian behavior of the protein motions probed by Elastic Incoherent Neutron Scattering (EINS). The combined theory displays a dynamical transition caused by the softening of few "torsional" modes in the low frequency regime ( $< 50\text{cm}^{-1}$  or  $< 6\text{meV}$  or  $> 0.6\text{ps}$ ). These modes change from Gaussian to a classical distribution upon heating. Our theory provides an alternative way to understand the microscopic origin of the protein dynamical transition.

---

\*ewp@purdue.edu

# 1 Introduction

Protein function is determined by both structural stability and flexibility. The stability is needed to ensure appropriate geometry of the protein, while the flexibility allows function to proceed at an appropriate rate. Quantitative measurements of the temperature dependent atomic mean square displacements (MSD) are possible by neutron scattering [1] [2][11] and Mössbauer absorption [8, 9, 10]. All of these experiments show a "dynamical transition" in hydrated proteins, which is marked by an abrupt MSD increase in the temperature range 160–240K. It is believed that this dynamical transition is correlated with protein function. Three prominent examples are the myoglobin-CO binding kinetics [12], electrostatic relaxation in green fluorescent protein [13], and the Arrhenius behavior of the electron transfer rate above the dynamical transition temperature. However, the time scale and the forms of the functionally important atomic modes remain a subject of active discussion [5][6][7].

Numerous theoretical studies of protein dynamics have been carried out by molecular dynamics (MD) simulations [14, 15, 16, 17] and normal mode analysis (NMA) [16, 18, 19, 20, 21]. NMA requires the use of Maxwell-Boltzmann or Gaussian distributions to describe the probability distributions of individual atoms or chemical bonds. Recently, several authors focused on the study of the non-Gaussian behavior of the total elastic incoherent neutron scattering (EINS) profile from a protein above dynamical transition temperature [4, 22, 25]. It should be noted that the distribution of all-atom MSDs from an EINS profile can still be non-Gaussian even if all atoms individually exhibit Gaussian dynamics. The Gaussian distribution, which is the ground state probability distribution for the quantum harmonic oscillator, is an appropriate approximation when  $\hbar\omega > kT$  ( $\omega > 200\text{cm}^{-1}$ ). In the Gaussian distribution, the atom has maximum probability in the equilibrium position. We find that in all self consistent theories, the use of a Gaussian distribution results in a molecular structure that will tend to be more rigid than what would be found by a more exact quantum approach. From Newton's second law, the classical harmonic oscillator (low frequency) has highest probability at the edges of the well because the atom moves most slowly near the classical turning points, which is contrary to the Gaussian or ground state probability distribution. The exact quantum behavior of low frequency modes would approach the classical displacement. In this paper we explore the role of incorporating the higher quantum vibrational states. This shows a softening of the structure in the correct temperature range.

The material studied by SCNMA is six-coordinate heme c type cytochrome f [26]. The iron normal modes are compared with the Nuclear Vibrational Resonance Spectroscopy (NRVS) spectrum [29]. NRVS is uniquely capable of displaying the low frequency vibrational displacement

spectrum of the Fe atom at the center of the heme as it sees all modes and can give quantitative values for displacements. It is then possible to define low frequency heme modes that are in agreement with observation with greater accuracy. This is a much more stringent test than most Raman comparisons as Raman displacements cannot be calculated with any accuracy.

SCNMA incorporates non-linearity into harmonic calculation by thermal-statistically averaging the curvature of the bond potential energies. Because vibrational modes that are not overdamped are detected by Raman and IR, one expects the effective Hamiltonian to be approximately harmonic. SCNMA should therefore be a valid approach. The SCNMA formulation arises from a variational procedure that finds the best effective harmonic Hamiltonian by minimizing the free energy. This method is described in detail elsewhere[31]. It has been successfully employed on models with multiple hydrogen stretching bonds such as the helix melting, conformational change in DNA and drug-helix stability, etc [32]-[35]. In those papers a Gaussian distribution was used to describe the displacement distribution. In this paper, we will further develop this method to incorporate non-Gaussian distributions into our calculation.

## 2 Quantum Harmonic Oscillator (QHO) theory applied to internal atomic bonds

### 2.1 The displacement distribution of the internal atomic bonds

For a bio-molecule with  $N$  atoms and  $M$  internal atomic bonds  $M$  is much larger than  $N$ . Standard NMA will give us  $3N-6$  non-zero normal modes. Their frequencies can be written as  $\omega = [\omega_1, \omega_2, \dots, \omega_{3N-6}]$ . The total MSD for frequency  $\omega$  can be written as

$$\langle \sum_{i=1}^n m_i r_i^2 \rangle = \frac{\hbar}{2\omega} \coth\left(\frac{\hbar\omega}{2k_B T}\right) \quad (1)$$

Subsequently, the temperature dependent total mean square amplitude for the one single internal bond is the sum of all normal mode amplitudes, which can be written as

$$D^2 = \sum_{\omega} D_{\omega}^2 = \sum_{\omega} d_{\omega}^2 \coth\left(\frac{\hbar\omega}{2k_B T}\right) = \sum_{\omega} \coth\left(\frac{\hbar\omega}{2k_B T}\right) |s_{\omega}|^2 \quad (2)$$

where  $D^2$  is the total mean square amplitude over all frequency modes,  $D_{\omega}^2$  is the mean square amplitude contribution and  $d_{\omega}^2$  is the zero point mean square amplitude for frequency  $\omega$ , and  $|s_{\omega}|^2$  is the projection of the normalized eigenvectors at eigenvalues (frequency)  $\omega$  onto the mass-weighted

internal coordinates. These amplitudes can represent a linear distance (for stretching bond) or an angular twisting (for angle bend and dihedral bond).

From QHO theory, the harmonic displacement distribution for one particular internal bond at frequency  $\omega$  can be written as

$$\langle u_\omega | H | \Psi_n \rangle = \sqrt{\frac{1}{2^n n!}} \left( \frac{1}{2\pi d_\omega^2} \right)^{1/4} e^{-\frac{u_\omega^2}{4d_\omega^2}} H_n \left( \sqrt{\frac{1}{2d_\omega^2}} u_\omega \right) \quad (3)$$

where  $u_\omega$  is the displacement variable for mode  $\omega$ ,  $H_n$  is the Hermite polynomial, and  $\Psi_n$  is the probability distribution for the  $n^{\text{th}}$  excitation state. Here we note that the ground state  $\langle u_\omega | H | \Psi_0 \rangle$  is in fact a Gaussian. The corresponding quantized energy levels are

$$E_n = \hbar\omega \left( n + \frac{1}{2} \right) \quad (4)$$

From the Boltzmann distribution, the displacement distribution of this internal coordinate for mode  $\omega$  can be written as

$$f_\omega(u_\omega) = \frac{\sum_{n=0}^{\infty} e^{-\frac{\hbar\omega(n+\frac{1}{2})}{kT}} \langle u_\omega | H | \Psi_n \rangle^2}{\sum_{n=0}^{\infty} e^{-\frac{\hbar\omega(n+\frac{1}{2})}{kT}}} \quad (5)$$

The joint probability density function for  $\omega = [\omega_1, \omega_2, \dots, \omega_{3N-6}]$  can be subsequently written as

$$g(u_{\omega_1}, u_{\omega_2}, \dots) = \prod_{\omega} f_\omega(u_\omega) \quad (6)$$

The total displacement is  $u = \sum_{\omega} u_\omega$ . Using a transformation of variables

$$[u = \sum_{\omega} u_\omega, u_{\omega_2} = u_{\omega_2}, u_{\omega_3} = u_{\omega_3}, \dots] \quad (7)$$

the total displacement distribution can be obtained as

$$f(u) = \int_{-\infty}^{\infty} \cdots \int_{-\infty}^{\infty} g\left(u - \sum_{j=2}^{3N-6} u_{\omega_j}, u_{\omega_2}, u_{\omega_3}, \dots\right) du_{\omega_2} du_{\omega_3} \cdots u_{\omega_{3N-6}} \quad (8)$$

To reduce unsystematic errors,  $u_{\omega_1}$  is chosen to have the largest amplitude of the  $3N - 6$  modes. Equation 8 requires  $3N - 7$  integrals of a  $3N - 6$  multi-variable function to calculate the actual displacement distribution of one single internal bond. For one standard NMA calculation,  $(3N - 7) \times M$  integrals are solved. To reduce the required calculation time, approximation methods are employed, as introduced in the next section.

## 2.2 The displacement distribution for single frequency harmonic motion and an approximation method

To understand the approximate temperature and frequency behavior of non-Gaussian distributions, that of a single frequency normal mode displacement is shown in Fig 1. It shows the temperature dependent single frequency displacement distribution at 300K for (a)  $\omega < 50\text{cm}^{-1}$  ( $> 0.67\text{ps}$ ), (b)  $50\text{cm}^{-1} < \omega < 80\text{cm}^{-1}$  (0.42ps-0.67ps), and (c)  $\omega > 80\text{cm}^{-1}$ .

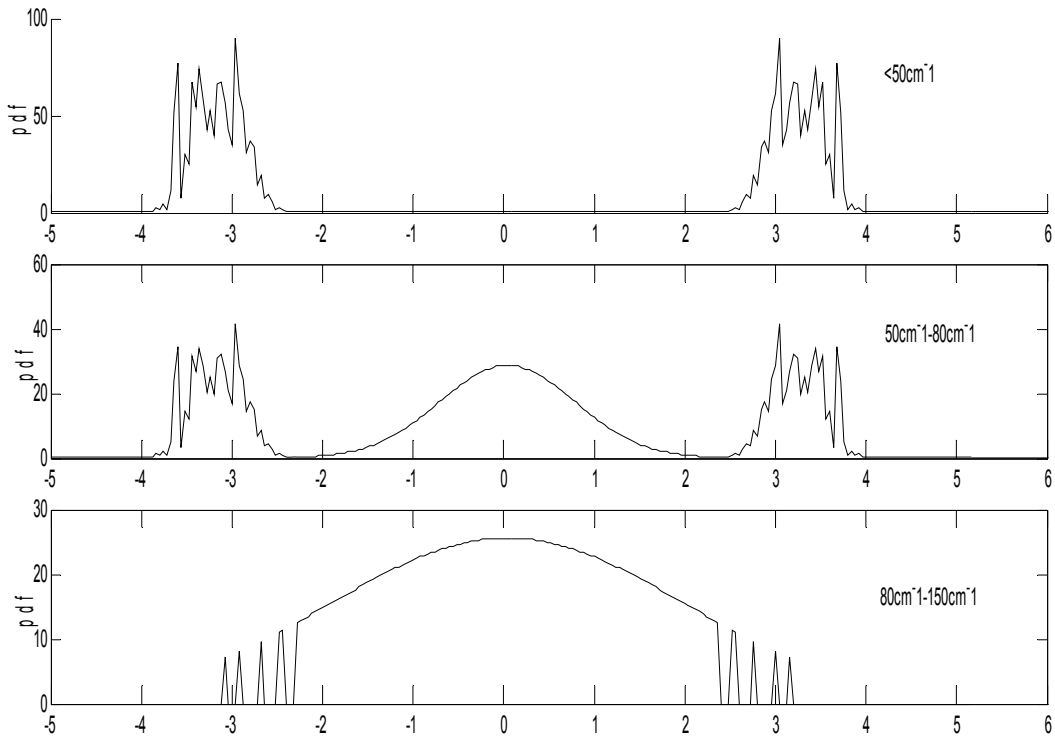


Figure 1: Characterization of the single frequency displacement distribution at 300K In (a) the displacement is similar to the classical distribution, (c) the displacement distribution is similar to a Gaussian, and (b) is a cross between the two

Fig 1 shows the displacement probability for a single frequency, but the displacement for a single bond is a superposition of many such frequency contributions with different amplitudes. The spread in amplitudes comes from the projection factors ( $|s_\omega|^2$ ) from equation (5) which come from the eigenvectors of the various modes. Even for low frequencies, any bond amplitude would be the sum of many distributions like those in Fig 1, all at different amplitudes from the origin. The central Limit Theorem (CLT) supposes that a large sum of this kind will add up to a Gaussian

distribution. This assumption has been central to all previous calculations using SCNMA. The situation could be quite different, however, if only a few low frequency modes dominate in the displacement of particular bonds. In such a case, for some range of temperatures, the displacement probability could resemble the plot in Fig 1-(a). We emphasize that the hydrogen bond stretching modes are typically above  $100\text{cm}^{-1}$  and fall into the Gaussian distribution regime. The bond modes that are softer than the hydrogen stretching bonds, i.e. the torsional motions, may exhibit non-Gaussian behavior at physiological temperature. All proteins have torsional modes and this effect may be manifested in many proteins.

From equation (5), the displacement distribution of the single frequency mode is approximately Gaussian when

$$\omega(T) > 0.27T\text{cm}^{-1}(\text{TinKelvin}) \quad (9)$$

and more classical when

$$\omega(T) < 0.17T\text{cm}^{-1}(\text{TinKelvin}) \quad (10)$$

From equations (9) and (10), the single frequency mode in the frequency regime  $< 50\text{cm}^{-1}$  (or  $< 6\text{meV}$  or  $> 0.7\text{ps}$ ) will transition from a Gaussian to a more classical distribution upon heating from low temperature to room temperature. It should be noted that the prominent "Boson peak" ( $1 - 3.5\text{meV}$  or  $10 - 30\text{cm}^{-1}$ ) from neutron scattering [3, 11, 36] or the "doming mode" from NRVs [29] and IR [44] experiments lie in this frequency regime.

To simplify the calculation, we use the assumption that the sum of the independent Gaussian variables is still a Gaussian and we treat all the normal modes above  $80\text{cm}^{-1}$  as one Gaussian distribution. Based on CLT, we can further simplify the low frequency displacement distribution calculation. If the displacement  $u$  for one internal bond is comprised of many low frequency modes, we can treat it as a Gaussian. To test how many significant low frequency ( $< 80\text{cm}^{-1}$ ) modes are needed to be able to use the Gaussian approximation without loss of accuracy, several NMA and subsequent displacement distribution calculations were run on the heme core. We found less than 5% deviation from Gaussian in the distribution of  $u$  (equation 8) when  $u$  has more than 5 low frequency modes each accounting for more than 10% of the total potential energy. Implementing these two approximations reduce our calculation time by a factor of more than 100.

### 3 Method

An initial classical NMA calculation was performed on the six-coordinate heme c type cytochrome f using the CHARMM force field [27, 28]. An all-atom model [28] was constructed from the X-

ray coordinates (PDB identifier 1EWH [26]). The model was subjected to force field minimization until the root mean square gradient of the potential energy was less than 0.0001 prior to performing a standard normal mode calculation with the VIBRAN facility in CHARMM[27].

The low temperature CHARMM force field was refined by comparison with the Nuclear Vibrational Resonance Spectroscopy (NRVS) spectrum[29]. The method of force field refinement process was described elsewhere[37, 38, 39]. The anharmonic functional forms were chosen from reference [40], in which Morse function, harmonic cos function and dihedral cos function were used to describe bond stretch interactions, angle bend interactions and torsional bond interactions. The resulting low temperature force constants can then be used along with data on atom distances and bond strength to fit anharmonic potential parameters. SCNMA was employed to allow exploration of temperature dependent changes in force constant and thermal expansion effects[31]. This method has been described in detail elsewhere[31, 32, 33, 34, 35], where the Gaussian approximation was used for the displacement variable  $u$ . The only difference here from the previous SCNMA is the explicit inclusion of non-Gaussian distributions for low-frequency modes. Here, we give a brief description of the computation:

- Input the effective force constants (the 1<sup>st</sup> iteration uses the force constants refined to experimental data) into the NMA and find the initial normal mode eigenvalues and eigenvectors.
- Calculate each internal coordinate's total mean square amplitude  $D^2$  and each normal mode contribution  $D_\omega^2$
- Calculate each internal coordinate displacement distribution  $f(u)$
- Calculate a new set of the effective force constants.
- Iterate to self consistency.

The calculation converged within 20 iterations.

## 4 Result and discussion

Fig 2 shows the comparison between the iron Vibrational Density Of State (VDOS) obtained from classical NMA and the NRVS experimental results. Good agreement is achieved over a wide range of frequencies, which indicates a useful choice for the low temperature limit force field. Here, we give a summary of the general results: (1) below  $80\text{cm}^{-1}$  are mostly iron-out-of-plane motions;

(2) the  $80 - 300\text{cm}^{-1}$  region has both iron in-plane and out-of-plane features; and (3)  $> 300\text{cm}^{-1}$  are mainly iron in-plane motions. If the calculations did not include anharmonic effects, the total displacements would be linear in temperature. Classical NMA results show that at low temperature ( $< 150\text{K}$ ), the iron out-of-plane MSD is about three times the iron in-plane MSD despite the fact that the iron in-plane motion has two degrees of freedom versus the single degree of out-of-plane motion.

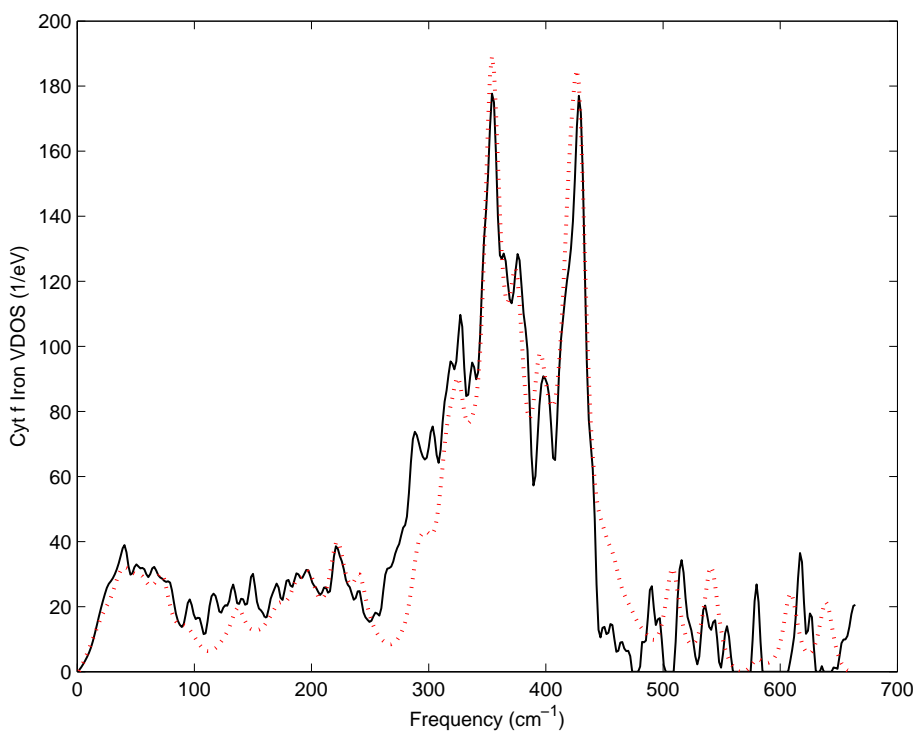


Figure 2: Comparison of the experiment (from reference [30]) and theoretical (from classical NMA) cytochrome f iron Vibrational Density Of State (VDOS) Solid black line: experiment; dotted red line: theory

Fig 3 and Fig 4 show the cyt f iron total MSD from SCNMA. These results are in general agreement with the Mössbauer absorption experimental results conducted on other heme proteins. The high frequency ( $> 200\text{cm}^{-1}$ ) normal modes are softened on an average of 1 – 2%. This is because the high frequency normal modes are dominated by covalent stretching bonds which have



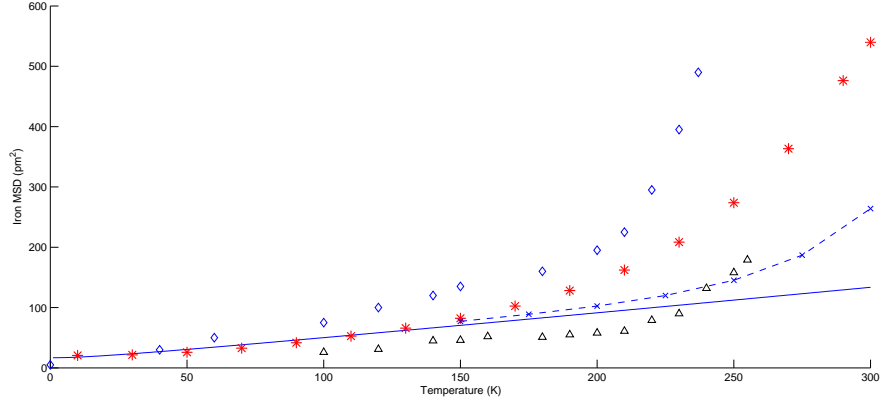


Figure 3: The iron MSD vs. temperature plot for various heme proteins. Blue line: iron MSD of cyt f by classical NMA; Blue cross and blue dashed line: iron MSD of cyt f from SCNMA with Gaussian distribution approximation. Red star: iron msd of cyt f from our SCNMA by implementing non-Gaussian displacement distribution. Blue diamond: iron MSD of myoglobin by Mössbauer absorption measurement from ref. [8]. Black upper triangle: iron MSD of cyt c by Mössbauer absorption measurement from ref. [9]

relatively larger strength and deeper potential wells. Moreover, these high frequency atomic motions follow a strict, narrow Gaussian distribution. Fig 4 shows that the iron dynamical transition is caused by iron low frequency out-of-plane motions. At lower frequency, the large iron out-of-plane motion becomes possible because of the small energy involved in changing the torsion angles. As temperature increases, more and more displacement will spread out from the Gaussian centroid. This low frequency classical behavior of the atomic displacement distributions coincides with the fact that the curvature of the potential function decreases over the distance from the centroid, which results in the abrupt MSD increase seen in our SCNMA model as compared with calculations implementing only Gaussian distributions (Fig 4).

To analyze the protein flexibility, the force strength defined by Zaccai [41] is generally used by other authors [42]

$$k_0 = \frac{k_B}{d \langle r^2 \rangle} \frac{d \langle r^2 \rangle}{dT} \quad (11)$$

From this definition, the iron force strength decreases by a factor of  $\sim 5-7$ . From NMA, the force constant is  $k_0 = m\omega^2$  and we extract  $\omega$  to find  $r^2$ . We found that the dihedral bonds, which are the major dynamical element contributing to the iron dynamical transition in our model, are softened

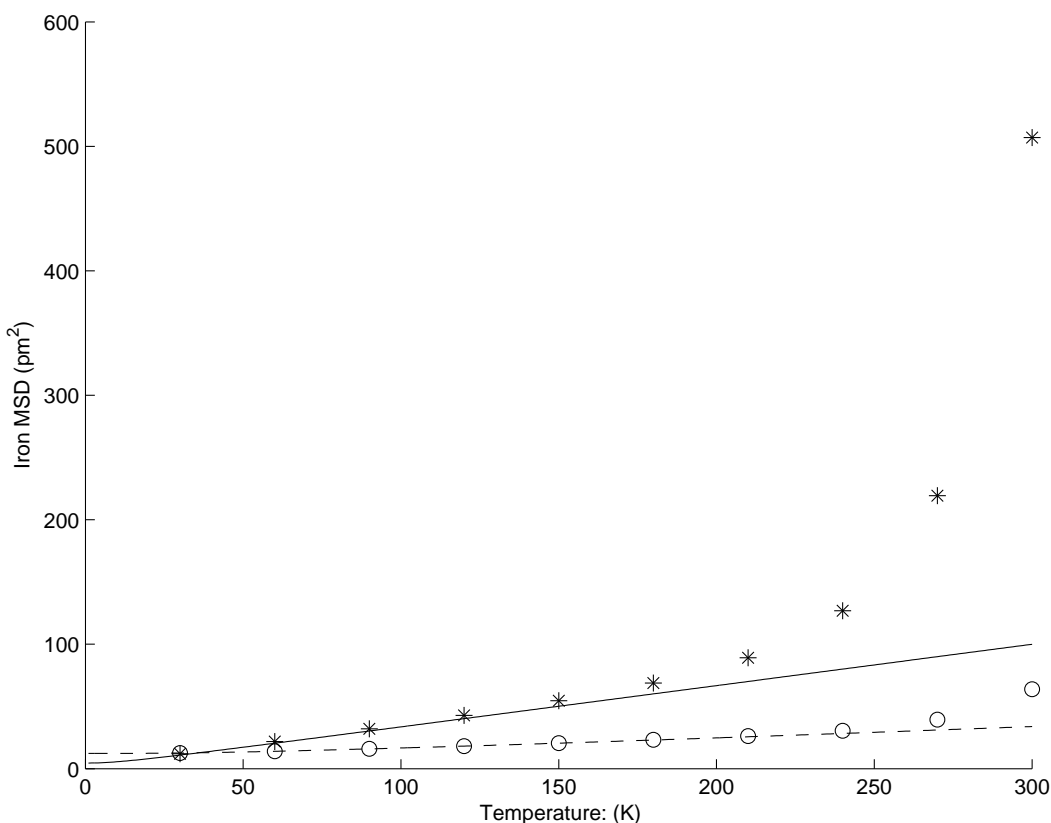


Figure 4: The cyt f iron in-plane and out-of-plane MSD from SCNMA. Dashed line: iron in-plane MSD from classical NMA; Circle: iron in-plane motion from SCNMA; Solid line: iron out-of-plane motion from classical NMA; Star: iron out-of-plane motion from SCNMA

by only  $\sim 20\%$ , as show in Table 1. The difference between the two definitions can be explained with equation 1. A simple plot of equation 1 (Fig 5) shows that  $r^2$  increases exponentially below  $50cm^{-1}$ . Our results show significant lowering of frequencies in this frequency region. Moreover, we found that atoms with internal coordinates associated with soft bonds exhibit a larger MSD increase than other atoms in one particular normal mode.

The MSD spread over frequency increases disproportionately upon heating, as shown in Fig 6. At temperatures below  $\sim 150$  K, the iron MSD for the normal mode frequencies that are below  $50cm^{-1}$  takes about 84% of the total iron MSD, while at 300K it increases to 92%.

Generally speaking, the normal modes that participate in biochemical reactions should have the largest motional amplitudes. The largest amplitude among the iron out-of-plane normal modes

Bond Type	<150K (mdyne*A/rad)	300K (mdyne*A/rad)	Percentage Softened
Fe-N-C-C	0.127	0.096	24.4%
N-Fe-N-C	0.135	0.111	17.9%
Fe-N-C (-C)	0.062	0.050	19.4%
N-Fe-N (-N)	0.098	0.072	16.3%

Table 1: The softening of the iron dihedral force constant from SCNMA

— normally characterized as the "doming mode" — has been intensively studied experimentally [43]-[46] and theoretically [47]-[50]. This mode is Raman inactive in a four-fold symmetric porphyrin. The IR spectroscopy and NRVS of cytochrome f failed to identify a well-resolved mode with such character, and with the intensity expected for a heme doming mode in the low frequency region. The modes around  $40\text{cm}^{-1}$  and  $80\text{cm}^{-1}$  have been assigned to have the doming features by various authors [46][49][51]. In our SCNMA calculation, the normal modes around  $80\text{cm}^{-1}$  have the features of both iron doming motions and in-plane motions. The iron MSD in the frequency regime  $70 - 90\text{cm}^{-1}$  takes less than 10% of the total MSD, and these modes are close to Gaussian distributions at room temperature from QHO theory. A theoretical study of the doming mode has been carried out earlier by Li and Zgierski [47] on a five-coordinated heme model. In the study, the doming mode was predicted to be around  $50\text{cm}^{-1}$  and was calculated to be  $35\text{cm}^{-1}$ . Their analysis found that the doming mode takes about 90% of the iron MSD at room temperature. In one previous NMA calculation, one  $37\text{cm}^{-1}$  doming mode was found in four-coordinate heme compound Fe(OEP), which takes 67% of the total iron MSD (unpublished results). In our six-coordinate cytochrome f SCNMA, three normal modes that have the most iron MSD are ( $19\text{cm}^{-1}$ ,  $35\text{cm}^{-1}$  and  $49\text{cm}^{-1}$ ) at low temperature and softened to ( $14\text{cm}^{-1}$ ,  $23\text{cm}^{-1}$  and  $37\text{cm}^{-1}$ ). These three modes take 63% of the iron MSD and increase to 81% at room temperature. We assign them to the doming modes due to their significant doming features. QHO theory indicates that these modes are Gaussian distributions at low temperature ( $< 100\text{K}$ ) and more classical at room temperature (300K). As temperature increases, these modes develop other features like saddling and ruffling due to the softening of the dihedral bonds that are associated with these modes. The energy distribution shows that these doming modes are highly delocalized, i.e., the potential energy is distributed among a large num-

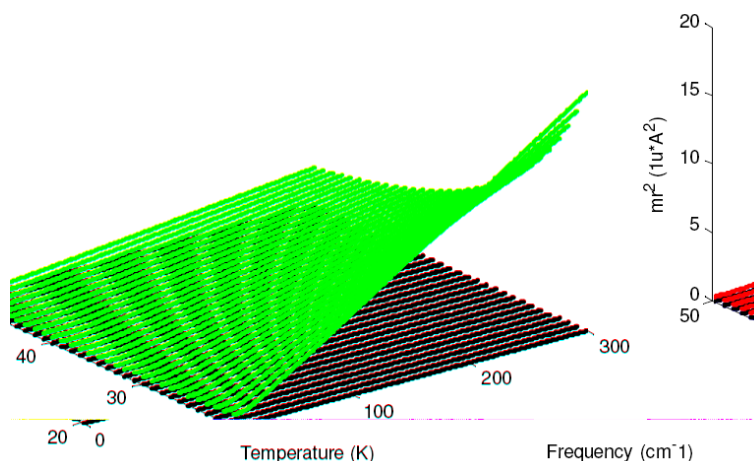


Figure 5: A plot of  $\langle \sum_{i=1}^n m_i r_i^2 \rangle$  as a function of temperature (T) and (low) frequency  $\omega$  from equation (4)

ber of internal coordinates and the kinetic energy is distributed among a large number of atoms. We also observe that the iron low frequency motions are in phase with some other soft bond atoms.

Besides the doming mode, some other significant water-protein motions are observed in the frequency regime below  $50\text{cm}^{-1}$ . These modes are softened by 20 – 50% from low temperature to room temperature. These results can also qualitatively explain the two onsets of anharmonicity suggested by several authors [5] [52] as they proposed there are two motional components: one happens at T 100K and one at T 200-230K. As shown in Fig 6, lower frequency modes have a relatively lower dynamical transition temperature.

The statistical properties of fast hydrated protein motions have been analyzed by neutron scattering [4] and X-ray diffraction experiments[6]. At temperatures below 200K, the displacement distribution is statistically a Gaussian. However, a deviation from a Gaussian distribution becomes significant at temperatures above 240K. In our SCNMA calculation, below 100K, the motions of individual atoms exhibit Gaussian behavior, but starting from 100 K, the atoms participating in soft internal coordinates transition from Gaussian to classical distribution upon heating. The percentage of heavy atoms that exhibiting classical behavior rises to 20% at 300K. This result agrees with the proposal by other authors who suggest the protein dynamical transition is caused by water induced torsional jump[4][11]. Furthermore, we also quantitatively identify that the normal modes that contribute to the dynamical transition lie in the frequency regime of  $< 50\text{cm}^{-1}$  at temperatures below the dynamical transition temperature.

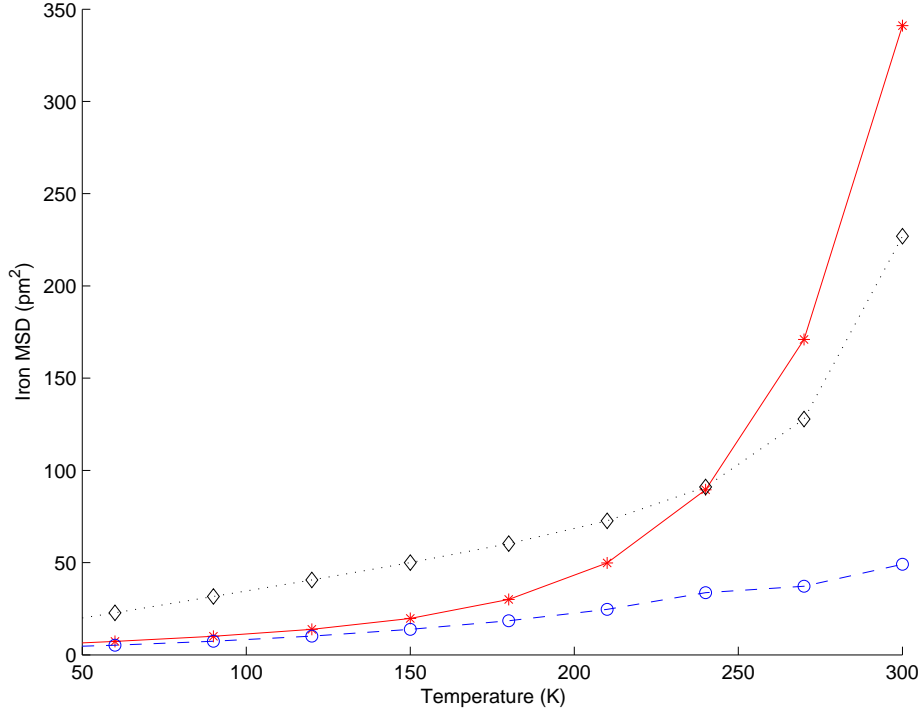


Figure 6: Cyt f iron MSD from SCNMA in three frequency regimes: (a) red star  $< 20\text{cm}^{-1}$  ( $2.5\text{meV}$ ), (b) black diamond:  $> 20\text{cm}^{-1}$  ( $2.5\text{meV}$ ) and  $< 50\text{cm}^{-1}$  ( $6\text{meV}$ ) and (c) blue circle  $> 50\text{cm}^{-1}$  ( $6\text{meV}$ )

## 5 Conclusion

SCNMA can be used to study temperature dependent protein vibrational motions. In the past, all such calculations assumed Gaussian displacement distributions. However, single oscillators depart from Gaussian distribution at higher temperatures. This departure from Gaussian behavior was studied quantitatively here using QHO theory and SCNMA. Our study of heme c type cytochrome f has led us to identify some specific features of the atomic interactions which may be of general validity. Our results show that only a few normal modes account for most of the motional amplitudes of a significant set of bonds. These modes lie in the frequency regime  $< 50\text{cm}^{-1}$  (or  $< 6\text{meV}$  or  $> 0.6\text{ps}$ ). The higher frequency normal modes essentially maintain a narrow Gaussian distribution. Above 100K, the low frequency modes transition from Gaussian to

more classical distributions upon heating, facilitating the softening of dihedral (torsional) bonds, which seems to lead to the dynamical transition.

## References

- [1] Wolfgang Doster, Stephen Cusack and Winfried Petry, *Nature* 337, 754 - 756 (1989).
- [2] W Doster, S Cusack, W Petry, *Phys. Rev. Lett.* 65, 1080-1083 (1990).
- [3] S. Cusack and W. Doster, *Biophysical journal* Volume 58, Issue 1, (1990).
- [4] Wolfgang Doster and Marcus Settles, *Proteins and Proteomics* Volume 1749, Issue 2, (2005).
- [5] Wolfgang Doster, *Eur Biophys J* 37:591-C602 (2008).
- [6] Dagmar Ringe, Gregory A. Petsko, *Biophysical Chemistry* 105 667-680 (2003).
- [7] S. Khodadadi, S. Pawlus, J. H. Roh, V. Garcia Sakai, E. Mamontov, and A. P. Sokolov, *J. Chem. Phys.* 128, 195106 (2008)
- [8] Chong SH, Joti Y, Kidera A, Go N, Ostermann A, Gassmann A and Parak F., *Eur Biophys J. Sep* 30(5):319-29 (2001).
- [9] E. N. Frolov, R. Gvosdev, V. I. Goldanskii, F. G. Parak, *JBIC* 2:710-C713 (1997).
- [10] Achterhold K, Keppler, C Ostermann, A. Van Bürck, U. Sturhahn W. Alp, E.E. Parak, F.G., *Physical Review E*, vol. 65, Issue 5, id. 051916 (2002).
- [11] M Ferrand, A J Dianoux, W Petry, and G Zaccai, *PNAS* vol. 90 no. 20 9668-9672 (1993).
- [12] W. D. Tian, J. T. Sage, V. Srajer, and P. M. Champion, *Phys. Rev. Lett.* 68, 408C411 (1992).
- [13] Van Thor, J., G. Y. Georgiev, M. Towrie, and J. T. Sage., *J. Biol. Chem.* 280:33652-C33659 (2005).
- [14] Jennifer A Hayward and Jeremy C Smith, *Biophysical Journal* Volume 82, Issue 3 (2001).

- [15] Jennifer A Hayward, John L Finney, Roy M. Daniel and Jeremy C Smith, *Biophysical Journal* Volume 85, Issue 2 (2003).
- [16] Alexander L Tournier and Jeremy C Smith, *PRL VOLUME 91, NUMBER 20* (2003).
- [17] Alexander L. Tourniera, Jiancong Xua and Jeremy C. Smith, *Biophysical Journal* Volume 85, Issue 3 (2003).
- [18] Nobuhiro Gō and Tosiyaaki Noguti and Testuo Nishikawa, *Proc Natl Acad Sci USA* 80(12):3696–3700 (1983).
- [19] Bernard R Brooks and Martin Karplus, *Proc Natl Acad Sci USA* 80(21):6571–6575 (1983).
- [20] B. Melchers, E. W. Knapp, F. Parak, L. Cordone, A. Cupane, and M. Leone, *Biophysical Journal* Volume 70 (2001)
- [21] K Hinsien and GR Kneller, *PROTEINS* (2008)
- [22] Hiroshi Nakagawa, Hironari Kamikubo, Itaru Tsukushi, Toshiji Kanaya and Mikio Kataoka, *J. Phys. Soc. Jpn.* 73 (2004).
- [23] H. Nakagawaa, A. Tokuhisab, H. Kamikubob, Y. Jotic, A. Kitaoc and M. Kataoka, *Materials Science and Engineering A*, (2006).
- [24] Atsushi Tokuhisa, Yasumasa Joti, Hiroshi Nakagawa, Akio Kitao, and Mikio Kataoka, *Phys. Rev. E* 75, 041912, (2007).
- [25] Hiroshi Nakagawaa, Hironari Kamikubob and Mikio Kataoka, (*BBA*) - *Proteins and Proteomics* (2009)
- [26] Carrell CJ, Schlarb BG, Bendall DS, Howe CJ, Cramer WA, Smith JL. *Biochemistry* Jul 27;38(30):9590-9 (1999).
- [27] Bernard R Brooks, Robert E Bruccoleri, Barry D Olafson, David J States, S Swaminathan and Martin Karplus, *J. Comput. Chem.* 4(2):187-217 (1983)
- [28] Alex D MacKerell, Jr, et al. *J Phys Chem B* 102(18):3586-3616, (1998).
- [29] W. Robert Scheidt Stephen M. Durbin, J. Timothy Sage, *Journal of Inorganic Biochemistry*, (2005).

- [30] K. L. Adams, S. M. Durbin et al, J. Phys. Chem. B, (2006).
- [31] E Prohofsky, Statistical mechanics and stability of macromolecules (1995).
- [32] Y Gao, K V Devi-Prasad, and E W Prohofsky, J Chem Phys (1984).
- [33] W. Zhuang, Y. Feng, and E. W. Prohofsky, Phys. Rev. A 41, 7033-C7042 (1990).
- [34] Y. Z. Chen and E. W. Prohofsky, Phys. Rev. E 49, 3444-C3451 (1993).
- [35] Earl Prohofsky, Bioelectrochemistry and Bioenergetics (1997).
- [36] Frick, B, Richter, D, Science 267, 5026 (1995).
- [37] Brajesh K. Rai, Earl W. Prohofsky, and Stephen M. Durbin, J. Phys. Chem. B, 109, 18983-18987, (2005).
- [38] Brajesh K. Rai, Stephen M. Durbin, Earl W. Prohofsky et al. J. Am. Chem. Soc., 125 (23), pp 6927C6936 (2003).
- [39] Timo E. Budarz, E. W. Prohofsky, and Stephen M. Durbin et al. J. Phys. Chem. B, 107 (40), pp 11170C11177 (2003).
- [40] Stephen L. Mayo, Barry D. Olafson, and William A. Goddard, J. Phys. Chem. 1990, 94, 8897-8909 (1990).
- [41] Giuseppe Zaccai, Science 2 June 288.5471.1604 (2000).
- [42] Bogdan M. Leu, J. Timothy Sage et al, Biophys J. 95(12):5874-89, (2008).
- [43] J. Timothy Sage, Stephen M. Durbin, Wolfgang Sturhahn, Sturhahn David C. Wharton, Paul M. Champion, Philip Hession, John Sutter, and E. Ercan Alp, Phys. Rev. Lett. 86, 4966C4969 (2001).
- [44] Dennis D. Klug, Marek Z. Zgierski, John S. Tse, Zhenxian Liu, James R. Kincaid, Kazimierz Czarnecki<sup>3</sup>, and Russell J. Hemley Dennis, PNAS (2002).
- [45] Flaviu Gruia, Minoru Kubo, Xiong Ye, Dan Ionascu, Changyuan Lu, Robert K. Poole, Syun-Ru Yeh and Paul M. Champion, J. Am. Chem. Soc., 130 (41), p 13810 (2008).
- [46] Flaviu Gruiaa, Minoru Kuboa, Xiong Yea and Paul M. Champion, Biophys J. 2008 Mar 15;94(6):2252-68, (2008).



- [47] Xiao-Yuan Li and Marek Z. Zgierski, *Chemical Physics Letters*, Volume 188, Issues 1-2, (1992).
- [48] Minoru Kubo, Flaviu Gruia, Abdelkrim Benabbas, Alexander Barabanschikov, William R. Montfort, Estelle M. Maes, and Paul M. Champion, *J Am Chem Soc.* 130(30):9800-11, (2008).
- [49] Pawel M. Kozlowski and Thomas G. Spiro Attila Beřces and Marek Z. Zgierski, *J. Phys. Chem. B*, 102, 2603-2608, (1998).
- [50] Pawel M. Kozlowski, Thomas G. Spiro, and Marek Z. Zgierski, *J. Phys. Chem. B* 2000, 104, 10659-10666, (2000).
- [51] Bogdan M. Leu, Marek Z. Zgierski, Graeme R. A. Wyllie, W. Robert Scheidt, Wolfgang Sturhahn, E. Ercan Alp, Stephen M. Durbin, and J. Timothy Sage, *J. Am. Chem. Soc.*, 126 (13), pp 4211C4227, (2004).
- [52] E. Cornicchi, M. Marconi, G. Onori, and A. Paciaroni 2006 *Controlling*, *Biophysical Journal* Volume 91 289C297, (2006).